

DYNAMIC-MECHANICAL ANALYSIS AND MECHANICAL PROPERTIES OF POLY (PHENYLENE SULFIDE) REINFORCED WITH CARBON NANOFIBERS

B. Ramón^[1], E. Zuza^[1], A. Torregaray^[1], A. Gómez^[1,2], J.R. Sarasua*^[1]

^[1]Dpto. Ingeniería Minera y Metalúrgica y Ciencia de los Materiales, Universidad del País Vasco-Euskal Herriko Unibertsitatea (EHU-UPV), Bilbao

^[2]Advanced Design&Analysis. IDOM Engineering and Consultancy. 48014, Bilbao

Email jr.sarasua@ehu.es

SUMMARY

The change of diameter length scale from micrometer to nanometer in carbon fibres provides opportunities for innovative approaches in the preparation and characterization of a new generation of composite materials. Poly (phenylene sulfide) (PPS) is a high performance semi-crystalline thermoplastic that *a priori* seems a good candidate to be strengthened by carbon nanofibers for engineering applications.

Keywords: CNF, thermoplastic, semicrystalline, confinement, dynamic mechanical analysis

1. INTRODUCTION

CNFs can be obtained by thermolysis of hydrocarbons like benzene or methane with the presence of a metallic catalyser around 1100°C [1-2]. The development of carbon nanofiber (CNF) composite materials provides a new and interesting alternative in regard to the use of traditional micron sized carbon fibers when it is aimed to improve the physical and mechanical properties of polymeric matrices for structural applications. Previous studies conducted on poly (ether ether ketone) (PEEK), polycarbonate (PC) or poly (ethylene terephthalate) (PET) have proved the validity of the nano-scale paradigm to improve the mechanical behaviour of engineering thermoplastics [3-6]

Conventional micron-sized carbon fibres have been applied in a wide range of applications in combination with polymeric matrices and particularly for high mechanical performance [7]. Compared to CNFs conventional micron-sized carbon fibres (CF) fabrication involves several steps, using either polyacrylonitrile (PAN) or pitch as starting materials, which increases their price and limits their application. As a comparison, CNFs are obtained by only one step which dramatically reduces their production cost.

The efficiency of CNFs as reinforcing material for composites as well as the ability to improve the mechanical, electrical and thermal properties of polymeric materials is not sufficiently determined, yet it is expected it will be lower than that of carbon nanotubes (CNTs). However, CNFs are obtained in a much higher yield than CNTs, which makes their production very attractive for the industry. Further benefits of CNFs are their better

availability and their lower price compared to CNTs which are decisive factors for the composite industry.

In this work PPS/CNF composites were prepared by melt mixing 0.3, 0.6, 1, 3 and 5 wt. % CNF with PPS and then conformed in sheet form by compression molding. The sheets were water quenched to initially prevent PPS crystallization and then thermally treated by annealing to develop crystallinity. Glass transition, crystallization and melting behavior were determined by differential scanning calorimetry (DSC). Mechanical properties were determined by tensile tests and dynamic mechanical analysis (DMA). The effect of thermal treatment and CNF content on PPS thermal and mechanical properties is discussed.

2. MATERIALS AND METHODS

Poly (phenylene sulphide) (PPS), Fortron®0320, was supplied by *Ticona Engineering Polymers*. Carbon nanofibers were supplied by *Grupo Antolín Carbon Nanofibras* (GANF, Spain). The structure of these fibers consists of a spiral alignment of a graphene layer along an axis forming an array of truncated cones with a wide hollow core [8]. CNF fibers were observed by AFM giving diameters ranging from 30 nm 300 nm, lengths longer than 30 µm and a proper dispersion into the PPS matrix.

PPS/CNF composites were prepared in a *Brabender Plasticorder PL 2000* by melt blending at 300°C during 20 min. Pure PPS and 0.3, 0.6, 1, 3 and 5 wt.% CNF composites were prepared and stored to avoid humidity. The materials were afterwards compression moulded in a *Dr Collin* press, in sheet form of 1 mm thickness, by melting at 300°C and subsequent rapid cooling in a water bath. Finally, the sheets were cut in the required dimensions for subsequent analysis and mechanical testing.

Differential scanning calorimetry (DSC) was conducted on a DSC 2920 from TA Instruments, calibrated with indium and under argon conditions, at a heating rate of 20 °C/min. The glass transition temperature (T_g), cold-crystallization temperature (T_c) and melting temperature (T_m) of PPS and those of the composite compositions were determined together with their corresponding crystallization and melting enthalpies (ΔH_c and ΔH_m). The crystalline fraction of PPS (χ_c) was determined by means of the following equation taking the value of the standard melting enthalpy for PPS $\Delta H_m^0 = 76.5$ J/g [9]. W_m is the weight fraction of the polymeric matrix in the composite.

$$\chi_c = \frac{\Delta H_m - \Delta H_c}{\Delta H_m^0 W_m} \quad (1)$$

Tensile tests were conducted in a Zwick Z010 universal testing machine according to a ISO 527 type 5A standard, at 23 °C and 5mm/min. Young's modulus (E), yield strength and strain (σ_y , ϵ_y) and stress and strain at break (σ_b , ϵ_b) were determined as the mean value of at least 5 determinations.

Dynamic mechanical analysis (DMA) of PPS and its CNF composites was conducted on rectangular specimens in shear mode at a heating rate of 3°C/min and a frequency of 1 Hz. Storage modulus (G'), loss modulus (G'') and loss tangent ($\tan \delta$) were determined between 0°C and 175 °C. A range of isothermal temperatures from -30°C below T_g to +30°C above T_g , every 3°C was also chosen to conduct the DMA at different frequencies. The time-temperature superposition principle was used to compose the master curve for PPS and to obtain the Angell's dynamic fragility parameter in the framework provided by the Williams-Landel-Ferry theory.

3. RESULTS AND DISCUSSION

DSC analysis

Figure 1 shows the DSC curves of unreinforced PPS as-quenched and after annealing at 1min, 5min and 15min. The heat capacity change denoting the glass transition in the quenched sample occurs at 90°C. This is followed by a cold crystallization at 133 °C and a melting endotherm at 285 °C; the analysis of the PPS quenched sample revealed the existence of a 14.5 % crystalline fraction. Annealing of PPS at 120 °C for 5 min. or higher times revealed a suppression of the cold crystallization peak and a broadening and increase of the T_g position of about 10 °C. The crystalline fraction determined from eq. 1 revealed a continuous increase with annealing time, from 14.5 % in the as quenched sample until reaching a plateau level at approximately $\chi_c = 43\%$ for annealing times higher than 5 min (Figure 2).

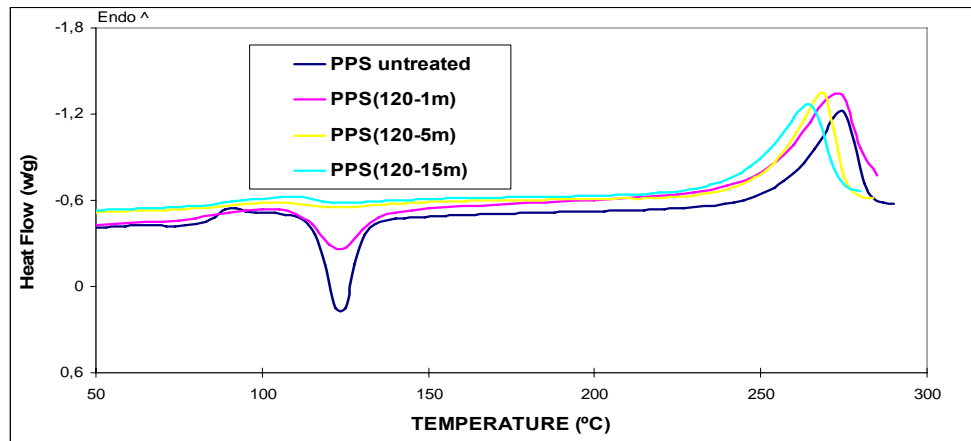


Figure 1 DSC curves at 10°C/min for neat PPS with different annealing times.

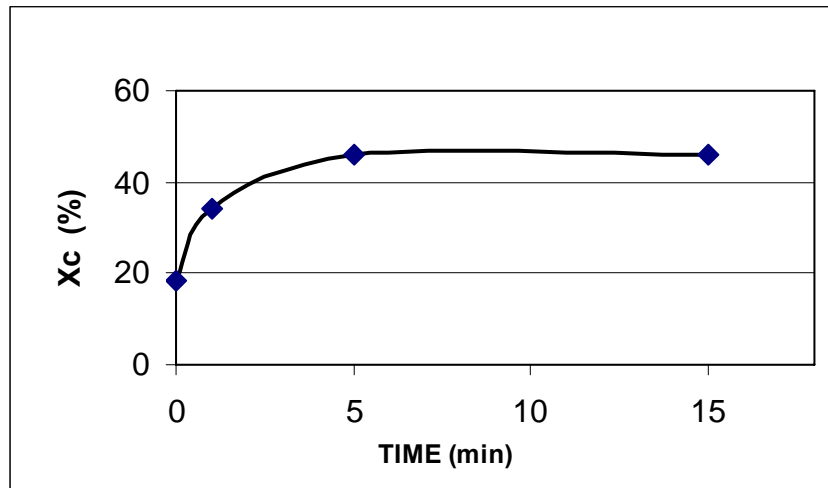


Figure 2. Evolution of PPS crystalline fraction (χ_c) with annealing time at 120°C.

The results of thermal parameters measured by DSC in pure PPS and its composites after quenching are presented in Table 1. It should be remarked here that the presence of CNF broadens the T_g transition increasing the value of T_g from 90 °C in neat PPS to 97.5 °C in its 5wt. % CNF composite. In addition a progressive reduction of cold crystallization (χ_{cc}) is observed suggesting that during conformation CNFs may be acting as nucleating agents of PPS crystallization. This observation is confirmed by the results obtained in crystalline fraction attaining $\chi_c=30\%$ for the as-quenched sample of 5 wt. % CNT, a value 50 % higher than that obtained in neat PPS after quenching.

Table 1 Thermal properties and crystalline fraction in PPS/CNF composites

MATERIAL	T_g (°C)	ΔH_m (J/gr)	ΔH_c (J/gr)	χ_c (%)	χ_{cc} (%)
PPS, unreinforced	90	34.6	23.5	14.5	30.7
PPS-1% CNF	96	34.1	15.8	24.1	20.7
PPS-3% CNF	97	32.6	12.6	26.9	16.5
PPS-5% CNF	97.5	30.9	8.6	30.6	11.5

Dynamic Mechanical Analysis

Figure 3 shows the dynamical mechanical curves of unreinforced PPS as quenched and after annealing for 1min, 5 min and 15min. At temperatures below its T_g PPS shows typical G' values corresponding to the glassy state of the polymer. It also shows increasing thermal stability for higher annealing times, which is attributed to the higher crystalline fraction developed during annealing. The $\tan \delta$ behaviour shows a double transition for the as quenched and the sample annealed for 1min, with a prominent dissipation first peak at 96.8 °C and a smaller second peak at about 120°C. However

PPS samples annealed longer than 5min show a single broadened glass transition with the dissipation peak centred at the same T_g position of the high temperature peak observed in low crystallinity samples. These results suggest the existence of a mobile and rigid amorphous fractions coexisting with the crystalline fraction in PPS.

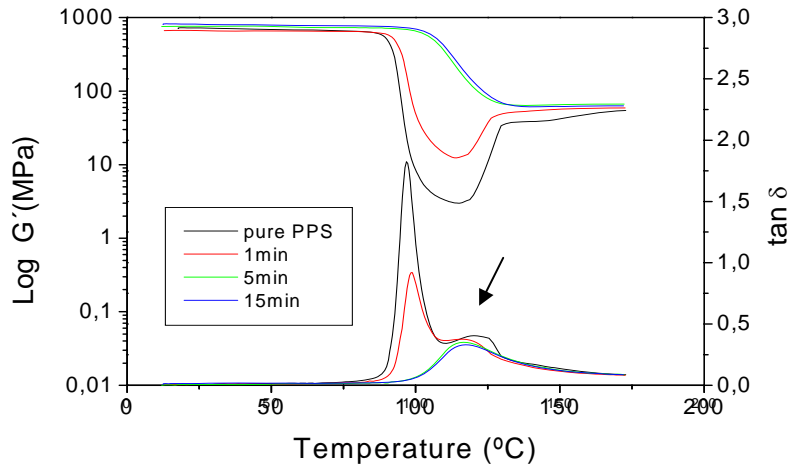


Figure 3. DMA curves of neat PPS before and after annealing at 120 °C.

Figure 4 shows the storage modulus and loss tangent evolution with temperature in PPS/CNF composites, as-quenched. Below T_g, PPS composites show increasing G' values with increasing CNF content, in regard to neat PPS. Additionally, the thermal stability of PPS around the T_g is radically improved since the fall of storage modulus at T_g is reduced not only because of the presence of a non dissipative CNF component in the composites but also by the CNF induced effect leading to crystalline fraction enlargement. The tan δ behaviour shows in composites a typical reduction in lost tangent peak values at T_g with increasing fiber compositions. This is attributed to the existence of a smaller amount of dissipative amorphous material composed of CNF and an enlarged PPS crystalline fraction derived from the nucleation effect of carbon nanofibers.

The tan δ behaviour in as quenched PPS composites also evidences double glass transition behaviour with a prominent dissipation peak around 100 °C and a smaller second peak around 125°C, yet the second peak decreases in height with increasing CNF contents and suppresses for compositions exceeding 1 wt.% CNF. These results should be interpreted by the rearrangement of a mobile and rigid amorphous fraction coexisting in PPS with a crystalline fraction and carbon nanofibers, the later two being components that do not participate in glass transition dissipative processes.

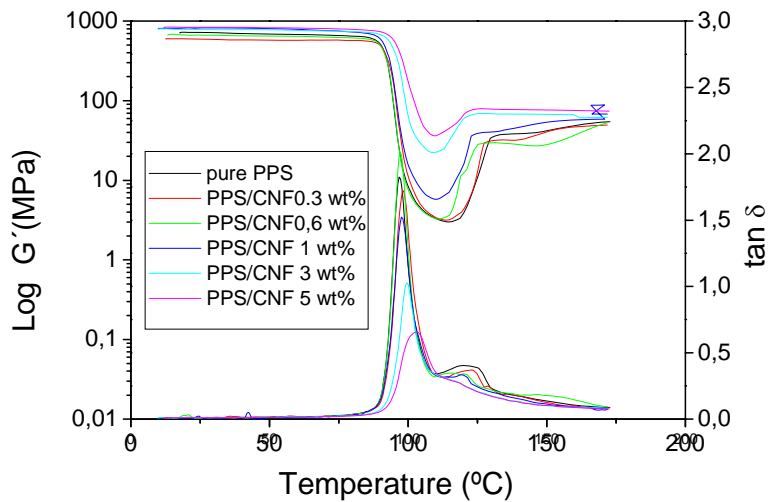


Figure 4. DMA curves of as-quenched PPS/CNF composites

Semicrystalline polymers for long time have been described consisting of two phases with different structures and properties. One of them is the crystalline phase, where molecules are arranged into lamellae further associated into larger objects, e.g. spherulites, and the other is the amorphous phase represented by disordered molecules or their parts situated in both inter-spherulitic and intra-spherulitic amorphous regions [10]. However it has been demonstrated in many polymers the existence of a third fraction denoted as a rigid amorphous fraction of the amorphous phase, RAF. RAF can be quantitatively determined by thermal calorimetric analysis since a deficiency in the difference in heat capacity, ΔC_p , at glass transition temperature is often observed indicating the existence of an amorphous phase not contributing to typical relaxation of chains [11].

Since macromolecules are longer than the thickness of the crystal lamellae, thus they can cross the phase boundaries and cause various degrees of coupling; on weak coupling, the dynamics of the non-crystalline segments shows usually a broadening of the glass transition region, yet on stronger coupling the non-crystalline material may also show a distinct glass transition, at a higher temperature of the bulk amorphous phase due to a rigid amorphous phase, and also a complete suppression of it if the cooperativity of chain motion is impeded when the dimension of the topological constraint (d) is smaller than the cooperative segment length (ξ) [12]. Restricted dynamics due to crystalline confinement and the presence of a rigid amorphous phase have been reported previously in semicrystalline polymers such as poly (phenylene sulphide) (PPS) [13,14], poly (ether ether ketone) (PEEK) [15], syndiotactic polystyrene [16], polycarbonate [17], or biodegradable poly (L-lactide) [18].

In this work two T_g dynamics were observed by DMA in PPS and its composites; the high T_g dynamics can be attributed to the hindered motions of the amorphous phase within the lamellar stacks (or within inter spherulitic regions) due to a rigid amorphous

phase; while the low T_g corresponds to the bulk like mobile amorphous phase. The progressive reduction of the high glass transition peak and the subsequent suppression for CNT compositions higher than 1 wt. % CNF suggests a strong interaction between CNF with RAF and MAF in PPS and a change in the dimension of the topological constraint (d) that attains a value smaller than the cooperative segment length due to an additional confining effect of carbon nanofibers.

Master curve of PPS and segmental dynamics around the T_g

The glass transition of supercooled polymer liquids is a kinetic process in which the relaxation time of the constituent molecules can increase by many orders of magnitude in a narrow temperature range. The glassy state is unstable because a glass is continually relaxing towards equilibrium and therefore the different related properties are also changing. The dynamic fragility [19] accounts for the ease with which the glass transition is completed. According to Angell [20], a polymer is defined dynamically fragile when there is little impediment for segmental relaxation of chains, carrying rapidly a drastic change in properties (viscosity, modulus, etc.) at the T_g . During the last years the fragility dilemma of liquids has raised research interests and particular efforts have been carried out to systematize the different polymers according to the fragility parameter [20-25].

Master curves were built for PPS using the DMA results obtained at different temperatures and frequencies, according to the WLF theory (equation 8). C_1 and C_2 constants were deduced by fitting the shift values (a_T) experimentally obtained to the

WLF equation 2: $\log \frac{\tau}{\tau_0} = \log a_T = \frac{-C_1(T - T_g)}{C_2 + T - T_g}$, where C_1 and C_2 are material

constants. Hence, the fragility parameter was determined as follows [14]:

$$m = \left. \frac{d(\log a_T)}{d(T_g/T)} \right|_{T=T_g} = \frac{T_g C_1}{C_2} \quad (\text{equation 3})$$

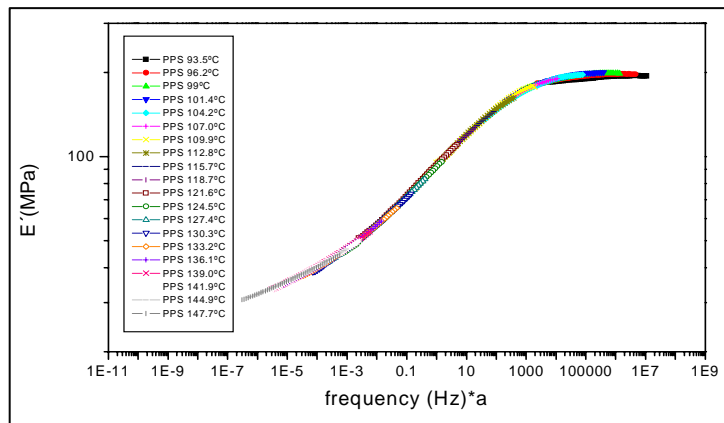


Figure 7. Master curve of unreinforced PPS. Frequency range at a given temperature: 20-0.01 Hz.

The dynamic fragility parameter of polymers has been reported to fall inside a $m=40$ -200 range [24]. If m has a high value, then the material is classified as a fragile liquid, whereas when m is low it is a strong glass former. Using the Williams-Landel-Ferry (WLF) equation to adjust the experimental values of Fig 7, a $m=84$ value was obtained. This relatively low value of the fragility parameter denotes a difficulty of PPS as a polymer glass former to change its conformational state and relax on cooling around the T_g as compared to other engineering polymers such as polyetherimide ($m=214$), polysulfone ($m=141$), or polycarbonate ($m=132$) [21].

Tensile behavior

Figure 5 shows the stress-strain behaviour of PPS and its CNF composites, as-quenched. The mechanical properties are presented in Table 1. Unreinforced PPS shows a typical tensile stress-strain curve of a ductile engineering polymer with a linear elastic region ($E=2.2$ GPa), yield point ($\sigma_y=50.2$ MPa) and an extensive deformation before break ($\epsilon_b=233.7$ %). Composites with 0.3 and 0.6 wt. % CNF show similar behaviour. However composites presenting 1 wt.% or higher CNF content present higher stiffness and show brittle behavior breaking just after the yield point.

Although the degree of dispersion of the nanofibres in the polymeric matrix and the adhesion of the nanofibres must be playing a role (Figure 8), the ductile-brittle transition in PPS/CNF composites could be explained in terms of confinement of PPS chains. In fact, the ductile-fragile transition occurs at 1 wt. %, a composition giving a suppression of the second T_g peak in DMA, hence it is proposed that carbon nanofibers and crystalline lamellae are acting as additional topological constraints suppressing the transition attributed to the rigid amorphous phase and restraining the shear deformation mechanisms needed for ductile behaviour.

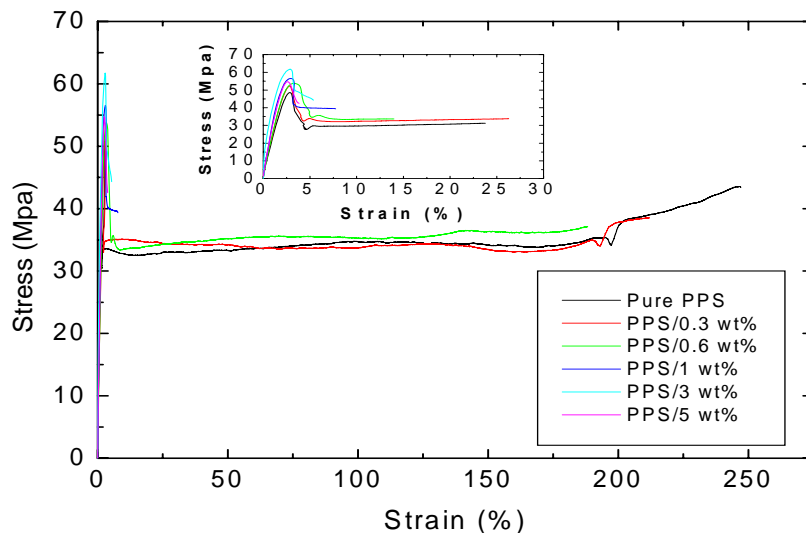


Figure 2. Stress-Strain curve for PPS/CNF composites with different compositions.

Table 2. Mechanical properties of PPS/CNF composites

Material PPS/CNF (wt. %)	E (GPa)	σ_y (MPa)	ϵ_y (%)	σ_b (MPa)	ϵ_b (%)
PPS/0	2.2 ± 0.2	50.2 ± 2.0	3.0 ± 0.2	39.4 ± 4.0	233.7 ± 33.0
PPS/0.3	2.2 ± 0.1	51.1 ± 1.0	3.2 ± 0.2	38.9 ± 1.3	212.7 ± 12.6
PPS/0.6	2.3 ± 0.1	53.9 ± 1.1	3.6 ± 0.2	40.8 ± 4.9	172.8 ± 90.0
PPS/1	2.7 ± 0.1	58.6 ± 3.4	3.3 ± 0.3	38.5 ± 2.0	6.9 ± 1.3
PPS/3	2.8 ± 0.2	61.0 ± 1.5	3.0 ± 0.2	47.6 ± 2.4	4.1 ± 1.8
PPS/5	2.7 ± 0.1	52.1 ± 2.2	2.5 ± 0.1	41.6 ± 3.7	5.5 ± 1.7

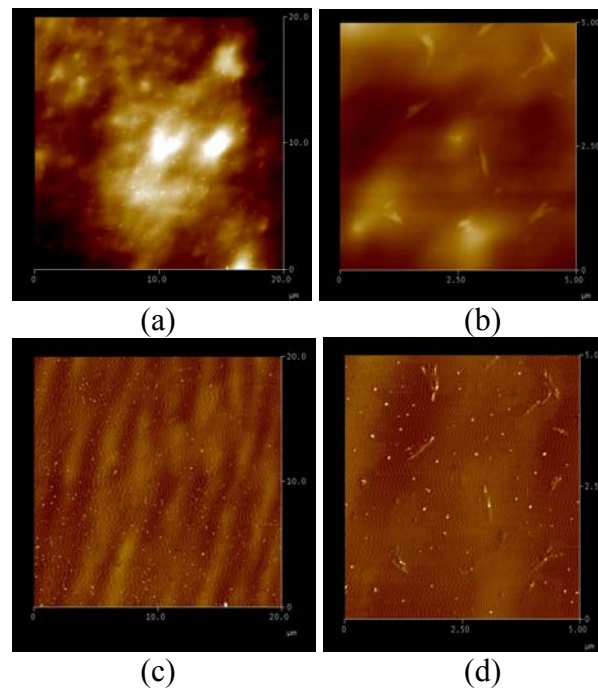


Figure 9. AFM image showing a good dispersion of CNF in PPS/1wt.% composite: a) height mode, 20 μm ; b) height mode, 5 μm ; c) phase imaging mode, 20 μm ; d) phase imaging mode, 5 μm .

ACKNOWLEDGEMENTS

The authors thank founding support from the European Community (Project FP7-NMP2007-Large 1-CP-IP 213939-1) and from the Basque Government Department of Education, University and Research (consolidated research groups GIC07/136-IT-339-07).

References

1. M. Endo, Y.A. Kim, T. Takeda, S.H. Hong, T. Matusita, T. Hayashi, and M.S. Dresselhaus, *Carbon*, **39**, 2010 (2001).

2. J.I. Paredes, A. Martinez – Alonso, and J.M.D. Tascon, *Carbon*, **39**, 1575 (2001).
3. J. Sandler, A.H. Windle, P. Werner, V. Altstadt, M. V. Es, and M. S. P. Shaffer, *Journal of Materials Science*, **38** 2135 (2003).
4. H. Ma, J. Zeng, M.L. Realff, S. Kumar, and D.A. Schiraldi, *Composites Science and Technology*, **63**, 1617 (2003).
5. Y.K. Choi, K.I. Sugimoto, S.M. Song, and M. Endo, *Material Letters*, **59**, 3514 (2005).
6. E.T. Thostenson, C. Li, and T-W Chou, *Composites Science and Technology*, **65**, 491 (2005).
7. J.R. Sarasua, P.M. Remiro, and J. Pouyet, *Journal of Materials Science*, **30**, 3508 (1995)
8. P.Werner, V.Altstadt, R. Jaskulka, O. Jacobs, J.K.W. Sandler, M.S.P. Shaffer, and A. H. Windle, *Wear*, **257**, 1014 (2004)
9. J.N. Hay, and D.A. Luck, *Polymer* **42**, 8301 (2001).
10. P. Slobodian, *J. Therm. Anal. Cal.*, **94**, 545 (2008)
11. D. Cangialosi, A. Alegría, J. Colmenero, *Europhys. Lett.*, **70**,:614 (2005)
12. B. Wunderlich, *Prog. Polym. Sci.*, **28**, 383 (2003)
13. S.X. Lu, P. Cebe, M. Capel, *Macromolecules*, **30**, 6243 (1997)
14. S.X. Lu, P. Cebe, *Polymer*, **37**, 4857 (1996)
15. A. Nogales A., T.A.Ezquerra, F. Batallan, B. Fric, E. Lopez-Cabarcos, F. J. Balta-Calleja, *Macromolecules*, **32**, 2301 (1999)
16. H. Xu, P. Cebe, *Polymer*, **46**, 8734 (2005)
17. E. Laredo, M. Grimau, A. Muller, A. Bello, N. Suarez, *Journal of Polymer Science Part B: Polymer Physics*, **34**, 2863 (1996)
18. E. Zuza, J. M. Ugartemendia, A. Lopez, E. Meaurio, A. Lejardi, J.R. Sarasua, *Polymer*, **49**, 4427 (2008)
19. C.A. Angell, *Journal of Non-Crystalline Solids*, **131**, 13 (1991)
20. C.A. Angell, *Science*, **67**, 1924 (1995)
21. D. Huang, G.B. McKenna, *Journal of Chemical Physics*, **114**, 5621 (2001)
22. R. Bohme, K.L. Ngai, C.A. Angell, J. Plazek, *Journal of Chemical Physics*, **99**, 4201 (1993)
23. I. M. Hodge, *Journal of Non Crystalline Solids*, **202**,164 (1996)
24. Q. Qin, B. McKenna, *Journal of Non Crystalline Solids*, **352**, 2977 (2006)
25. M. Arnoult, E. Dargent, J. F. Mano, *Polymer*, **48**,1012 (2007)